Phase-field simulation of abnormal grain growth during carburization in Nb-added steel

Takahisa Kinoshita[1] and Munekazu Ohno[2]

[1] Graduate School of Engineering, Hokkaido University, Kita 13 Nishi 8, Kita-ku, Sapporo, Hokkaido 060-8628, Japan

[2] Faculty of Engineering, Hokkaido University, Kita 13 Nishi 8, Kita-ku, Sapporo, Hokkaido 060-8628, Japan

Abstract:

Abnormal grain growth of austenite phase often takes place during carburization of steels, originating from carbon concentration dependence of pinning pressure of fine precipitates, the size of which is typically a few orders of magnitude smaller than the austenite grain size. In this study, the phase-field model for simulating the abnormal grain growth during carburization in steels is developed based on a mean field approximation in which the curvature-driven growth with the pinning pressure due to fine particles is reproduced by explicitly introducing the pinning pressure into the time evolution equations of order parameters. This model is applied to simulations of the austenite grain growth during carburization in Nb-added steels. Simulations are carried out to understand the occurrence of abnormal grain growth at different carburization temperatures for different steel compositions. In addition, an effect of non-uniform distribution of fine particles, which often appears as a consequence of microsegregation, on abnormal grain growth is investigated.

Keywords: phase-field model, carburization, abnormal grain growth, pinning effect, mean-field approximation

1. Introduction

Carburization is an effective way for improving wear resistance of surface of steels without deterioration of the fatigue property. Increasing of carburization temperature is one of important subjects for reducing the carburization time. For example, realization of carburizing depth of 1 mm in a steel requires a carburization process for 12 hours at 930ºC, while it can be reduced to only 3 hours at 1050ºC [1]. However, the increment of carburization temperature causes the occurrence of abnormal grain growth (AGG) in which some grains preferentially grow extremely large, consuming fine grains [1]. Since AGG leads to an increase of heat treatment distortion of products and decreases of the strength and toughness, it is necessary to suppress the occurrence of AGG. Hence, it is important to elucidate the mechanism and the conditions for the occurrence of AGG.

Fine precipitates in polycrystalline materials exhibit the pinning pressure on grain boundary migration of the matrix phase. The occurrence of AGG is closely related to the pinning effect [2-5]. The pinning pressure ΔP_{pin} is described as follows [3];

$$\Delta P_{pin} = \beta\sigma\frac{f_v}{r} \quad (1)$$

where β is a constant, σ is the grain boundary energy, f_v is the volume fraction of pinning particles and r is the radius of pinning particles. Since ΔP_{pin} depends on f_v and r, ΔP_{pin} is time-dependent when f_v and/or r change with time. Grain growth in steels can be effectively inhibited by carbides, nitrides and carbonitrides [4, 5]. In a steel with Nb addition which is our main concern in this paper, NbC phase works as a pinning particle and this pinning effect results in refinement of the austenite grain structure [2]. However, as the carbon concentration increases in the steel, the volume fraction of NbC first increases and then decreases according to the isothermal section of the phase diagram of Fe-C-Nb system at the carburization temperatures

[6]. During carburization, therefore, the dissolution of NbC in the austenite phase takes place and the pinning effect of NbC accordingly diminish, causing the occurrence of AGG [6]. It is important to clarify the condition of occurrence of AGG in steels. However, many factors such as carburization temperature, carburization time, solute concentrations and initial microstructure affect the occurrence of AGG, which makes it difficult to elucidate the conditions for occurrence of AGG in detail only by means of experimental techniques. Therefore, it is necessary to develop a simulation approach that can deal with AGG during carburization.

AGG has been investigated by using numerical simulations based on the Monte-Carlo method [7, 8] and the phase-field method [9, 10]. In particular, the phase-field method becomes an effective way for simulating various microstructural evolution processes because the diffuse-interface description of this method allows for simple computational algorithm and accurate computation of curvature effects [11, 12]. The pinning effect on grain growth has been described in the multi-phase-field method [9, 10, 13-16] in which a grain structure is described by a set of order parameters representing a probability of finding a grain and the grain boundary is characterized by spatial non-uniformity of the order parameters. In early studies on the pinning effect [9, 10, 13-16], the pinning particle is explicitly described in the microstructure by introducing an order parameter for the pinning particle phase. This method has successfully been applied to investigation of grain growth processes including AGG in various materials. However, a problem arises in the case of AGG in steels. Note that the spatial grid spacing in phase-field simulations is determined by the size of microstructure. Hence, the grid spacing must be very small when fine particles and/or fine grains exist in the microstructure. In case of AGG in steels, austenite grains are typically 10^{-5}-10^{-3} m in size, while the precipitates such as NbC are often 10^{-8}-10^{-7} m in size. Namely, there is a huge difference between the sizes of the

austenite grains and pinning particles. It is virtually impossible to simulate AGG in steels with the use of usual computational resources. To the best of authors' knowledge, AGG during carburization of steels has never been simulated by the phase-field models. It is also important to point out that the distribution of pinning particles is not always uniform. In particular, the microsegregation formed by solidification processes causes non-uniform distribution of pinning particles, thus affecting grain growth behavior and occurrence of AGG. The simulation for grain growth with non-uniformly distributed pinning particles must be conducted in extremely large computational system and it is virtually impossible because of the extremely large computational cost.

Recently, new phase-field methods have been developed for describing pinning effects [17, 18]. In these methods, the pinning pressure is calculated based on a mean-field approximation. To be more specific, the pinning particles are not explicitly described in the microstructure and, instead, the curvature-driven dynamics including the pinning effect is reproduced by directly introducing ΔP_{pin} into the time evolution equations of the order parameters. This approach allows for simulations of grain growth with pinning effect of extremely fine particles. In this study, this approach is extended to deal with AGG during carburization of steels. The main objective of this paper is to develop the phase-field method for AGG during carburization with the use of the mean field approximation of the pinning effect. We focus on a Nb-added steel and investigate the occurrence of AGG during carburization processes at different temperatures in steels with different compositions. Furthermore, simulations for AGG with non-uniform distribution of pinning particles are presented with an aim to demonstrate usefulness of the present approach.

2. Method

2.1. Multi-phase-field method

The phase-field method has been applied to simulations of various microstructural evolution processes [11, 12]. The multi-phase-field method is an effective method for calculating the grain growth in polycrystalline materials [19-21]. In the multi-phase-field method, the phase-field variable ϕ_i takes +1 in the grain i and 0 outside the grain i and it varies from +1 to 0 inside the grain boundary. The normalization condition $\sum_{i=1}^{N} \phi_i = 1$ is satisfied at every grid point. Here, N represents the total number of grains considered in the simulation. The time evolution equation of ϕ_i is given by [19, 20]

$$\frac{\partial \phi_i}{\partial t} = -\frac{2}{S}\sum_{j \neq i}^{N} s_i s_j M_{ij}\left[\frac{\delta F}{\delta \phi_i} - \frac{\delta F}{\delta \phi_j}\right] \tag{2}$$

where

$$\frac{\delta F}{\delta \phi_i} = \sum_{k \neq i}^{N}\left[\frac{\varepsilon_{ik}}{2}\nabla^2 \phi_k + \omega_{ik}\phi_k\right] \tag{3}$$

Here, s_i is the step function associated with ϕ_i, which takes 0 for $\phi_i = 0$ and takes 1 for $\phi_i > 0$. S is given as $S = \sum_{i=1}^{N} s_i$. M_{ij}, ε_{ij} and ω_{ij} are the phase-field mobility, the gradient energy coefficient and potential height, respectively, between the grains i and k. In this study, we assume isotropic grain boundary properties for simplicity. Therefore, $M_{ij}=M$, $\varepsilon_{ij}=\varepsilon$, $\omega_{ij}=\omega$ were employed in simulations. When the grain boundary energy and thickness are indicated by σ and W, respectively, ε and ω are given as $\varepsilon = 2\sqrt{2W\sigma}/\pi$ and $\omega = 4\sigma/W$. Equation (2) can reproduce the well-known relationship for the curvature-driven grain growth as follows [19],

$$v_{gb} = -m\sigma\kappa \tag{4}$$

where v_{gb} is the velocity of grain boundary, m is the grain boundary mobility and κ is the curvature of grain boundary. When the isothermal process is considered, the following relation is satisfied [19, 22, 23],

$$R^2 - R_0^2 = kt \tag{5}$$

where R is average radius of grains, R_0 is initial average radius of grains and k is a constant. This relationship holds true during the grain growth without pinning effect. Note that the constant k in Eq. (5) is the only input parameter for the isothermal grain growth. The temperature dependence of k for austenite grain growth was empirically determined in the previous work [24] and, therefore, it was employed in this study. The pinning effect is introduced into this multi-phase-field model based on the mean field approximation as detailed below.

2.2. Pinning force

In the present approach, the pinning particles are not explicitly described in the microstructure. Note that when the fine particle is densely distributed, the local pinning pressure given by Eq. (1) acts on moving grain boundary and, thereby, it can be directly introduced into the time evolution equation of ϕ_i. By including the pinning effect, the time evolution equation (2) is now rewritten for the case of $S = 2$ as follows [18],

$$\frac{\partial \phi_i}{\partial t} = M\left(\varepsilon^2 \nabla^2 \phi_i - \omega(1 - 2\phi_i) - \frac{8}{\pi}\sqrt{\phi_i(1-\phi_i)}G_{pin}\right) \tag{6}$$

where G_{pin} is given as

$$G_{pin} = \begin{cases} -\Delta P_{pin} & for\ \kappa > \Delta P_{pin} \\ \kappa & for -\Delta P_{pin} \le \kappa \le \Delta P_{pin} \\ \Delta P_{pin} & for\ \kappa < \Delta P_{pin} \end{cases} \tag{7}$$

where κ is the local curvature of grain boundary given by $\kappa = -\nabla \cdot \left(\frac{\nabla \phi_i}{|\nabla \phi_i|}\right)$ and ΔP_{pin} is given by Eq. (1). This model reproduces the well-known relationship in the theory of pinning effect as given by the following equation [18, 25],

$$v_{gb} = \begin{cases} -m(\sigma\kappa - \Delta P_{pin}) & for\ \sigma\kappa > \Delta P_{pin} \\ 0 & for -\Delta P_{pin} \le \sigma\kappa \le \Delta P_{pin} \\ -m(\sigma\kappa + \Delta P_{pin}) & for\ \sigma\kappa < -\Delta P_{pin} \end{cases} \tag{8}$$

For the sake of simplicity, we neglect the effect of pinning particles on motion of multiple junction of grain boundaries as commonly done in the theories of pinning effect.

The multi-phase-field model thus described can be extended to deal with the grain growth during carburization by introducing dependencies of the grain boundary energy, mobility and the pinning pressure on the carbon concentration. In this study, the grain boundary energy and mobility are assumed independent of carbon concentration for the sake of simplicity. Only the dependence of the pinning pressure on carbon concentration is considered. First, the pinning pressure given by Eq. (1) is extended to include effects of different pinning particles as follows [26],

$$\Delta P_{pin} = \beta\sigma \sum_{l} \frac{f_l}{r_l} \tag{9}$$

where f_l and r_l are volume fraction and radius of the pinning particle specified by the subscript l, respectively. f_l and r_l generally change with time and such time changes can be described using several theoretical models. In this study, it is assumed that f_l immediately takes the equilibrium value under the given carbon concentration. The time change of r_l is described by the following equation for the Ostwald ripening, [27],

$$r_l^3 - r_{l,0}^3 = k_l t \tag{10}$$

where $r_{l,0}$ and k_l are the initial average radius and a kinetic constant of the pinning particle l, respectively. The details of these parameters will be described in the next sub-section.

2.3. Computational conditions

Table 1 shows the composition of Nb-added steel of our focus. In this steel, the pinning effects due to NbC and AlN particles arise in the austenite grain structure. The diffusion of carbon from the surface into the steel was described by an analytical solution of Fick's second law with the fixed carbon concentration at the surface. We assumed NbC as the stoichiometric

compound and calculated the volume fraction of NbC, f_{NbC}, from the local concentrations of carbon and niobium using the following solubility limit in the austenite [6],

$$\log[Nb][C] = -\frac{5600}{T} + 1.74 + [C]\left(\frac{1380}{T} - 0.027\right) \quad (11)$$

where $[Nb]$, $[C]$ and T represents niobium concentration in austenite, carbon concentration in austenite and temperature, respectively. Therefore, f_{NbC} changes with time during carburization. The volume fraction of AlN, f_{AlN}, is calculated from the local concentrations of aluminum and nitrogen using the following solubility limit [28],

$$\log[Al][N] = -\frac{8296}{T} + 1.69 \quad (12)$$

In this approach, f_{AlN} is independent of carbon concentration and, accordingly, f_{AlN} does not change during carburization.

In the phase-field simulations, the pinning pressure ΔP_{pin} was calculated as follows. The volume fractions of NbC and AlN, f_{NbC} and f_{AlN}, are calculated from Eqs. (11) and (12), respectively. Also, the radii of these particles are calculated from Eq. (10) using the initial values $r_{NbC,0}$ and $r_{AlN,0}$. Then, the local value of ΔP_{pin} is calculated by substituting the values of f_{NbC}, f_{AlN}, r_{NbC} and r_{AlN} into Eq. (9). Therefore, ΔP_{pin} depends on the carbon concentration according to Eq. (11). For the sake of simplicity, the values of $r_{NbC,0}$ and $r_{AlN,0}$ were set to 10 and 40 nm, respectively, in the whole system at the beginning of all simulations.

In this study, we performed three types of simulations. The first one is the simulation of grain growth under the constant pinning pressure without the carburization, from which the average radius attained with complete pinning is investigated. The second one is the simulation of grain growth during the carburization at some different conditions. The last one is the simulation of grain growth during carburization in steels with non-uniform distribution of pinning particles. The microsegregation formed during the solidification often causes the non-uniform distribution of particles. An effect of such non-uniformity on the grain growth can be

considered in the present approach and it is included in the present simulation in a simple way that will be described later.

All calculations were performed in two-dimensional (2D) systems. The simulations for grain growth with the constant pinning pressure was conducted in 2D system of 1 × 1 mm^2 which was discretized into 2048 × 2048 grid points for the finite difference method. The periodic boundary condition was applied to all computational boundaries. The simulations for the grain growth during the carburization with uniform and non-uniform distribution of pinning particles were carried out in the 2D system of 0.5 × 1 mm^2 consisting of 1024 × 2048 grid points. The carburization occurs at $x = 0$. The Neumann boundary condition was applied to x-direction, while the periodic boundary condition was applied to y-direction.

In all simulations, the grain boundary thickness W was set to $W = 6\Delta x$ with the spatial grid spacing Δx. The initial grain structures in all cases were obtained by calculating microstructure evolution starting from randomly distributed grains in the initial matrix which has a higher energy than the grains. The active parameter tracking (APT) algorithm [19] was employed to save the computational cost. In the APT algorithm, the maximum number of stored phase-field variables in each grid points was set to 5. We accelerated the simulations by using a TESLA P100 graphics processing unit (GPU). All input parameters are listed in Table 2.

3. Results and discussion

3.1. Constant pinning force without carburization

We first carried out simulations for isothermal grain growth without the carburization to understand the behavior of average grain radius attained with complete pinning. For the sake of convenience, Eq. (1) is expressed as follows,

$$\Delta P_{pin} = \beta\sigma\frac{f_v}{r} = \frac{\sigma}{R_{pin}} \tag{13}$$

where R_{pin} is called the pinning radius in this paper.

Figure 1(a) shows the initial grain structure, the average grain size of which is about 10 μm. The initial value of total number of grains, N, is about 2×10^4 and the computational time was about 2.5 hrs. The grain structures after isothermal holding for t = 13 s at T = 1050°C are shown in Figs. 1(b) and (c). Figure 1(b) is the result without the pinning effect, i.e., R_{pin} = ∞. It shows the grain structure after normal grain growth where the grains uniformly grew. Figure 1(c) represents the grain structure calculated for R_{pin} = 90 μm. The average grain size in Fig. 1(c) is smaller than the one in Fig. 1(b) and it represents the pinning effect.

Figures 2(a) and (b) show the time changes of square of average grain radius during the grain growth processes with R_{pin} = ∞ and R_{pin} = 90 μm, respectively. The square of grain radius linearly increases with time in Fig. 2(a), as is consistent with Eq. (5). In Fig. 2(b), however, the grain radius takes an almost constant value after t = 6 s. Namely, the grain growth is suppressed due to the pinning effect.

We performed the same simulation for different values of R_{pin} using the different initial grain structures with initial average radius set to R_{ini} = 5, 10 and 15 μm. The summary of the results is shown in Fig. 3 where the horizontal axis is the pinning radius R_{pin}, while the vertical axis represents the final radius. The different symbols represent the data obtained from the initial grain structures with the different value of R_{ini}. It is first important to point out that all data can be well described by the single straight line regardless of R_{ini}. The slope of the straight line was calculated to be 0.67, while the slope is 0.5 in the Hillert's theory [24]. Our result is similar to the results of the model with double well potential, i.e., 0.73 in 2D simulation and 0.60 in 3D simulation [17]. From the results of simulations for isothermal grain growth without carburization, one can confirm that the pinning effect can be described in the present model.

3.2. Grain growth during the carburization

We focus on the grain growth during carburization. The microstructural evolution during the carburization process at T = 1050°C is shown in Fig. 4. The initial average radius of grains is R_{ini} = 10 μm. The initial value of total number of grains, N, is about 10^4 and this computation took about 21 hrs. The pinning radius R_{pin} corresponds to R_{pin} = 3.67 μm in the steel composition of Table 1. The carburization occurs from the left-side edge of the computational system, i.e., x = 0. As described above, the increase in carbon concentration causes the decrease in f_{NbC} in this steel and thereby the decrease in the pinning pressure. In Fig. 4, the grain growth accordingly takes place from the left-side edge, while the grain growth in the right-side region are completely suppressed due to the strong pinning effect of NbC. Some grains grew extremely large at t = 1500 s. Namely, AGG takes place during the carburization process.

Figures 5(a) and (b) show the spatial profiles of carbon concentration and pinning pressure of NbC, ΔP_{NbC}, respectively, at the different time steps in the simulation shown in Fig. 4. The carbon gradually diffuses into the steel and the pinning pressure ΔP_{NbC} accordingly changes with time. The spatial profile of ΔP_{NbC} is not monotonic. At t = 500 s, ΔP_{NbC} completely vanishes at x = 0 mm and it gradually increases from x = 0.08 mm, followed by the decrement from x = 0.28 mm. The value of ΔP_{NbC} at x = 0.5 mm is close to its initial value. This non-monotonic behavior of ΔP_{NbC} entirely originates from the concentration dependence of f_{NbC}. This profile is shifted toward the right-side region as the carburization proceeds. In short, ΔP_{NbC} gradually diminishes from the left-hand side and it causes the occurrence of AGG in Fig. 4. The positions where $\Delta P_{\mathrm{NbC}} = 0.25\Delta P_{\mathrm{NbC},ini}$ and $\Delta P_{\mathrm{NbC}} = 0$ are shown by the arrows in Fig. 4. Here, $\Delta P_{\mathrm{NbC},ini}$ is the initial value of ΔP_{NbC}. Since the pinning pressure due to AlN is relatively small in this steel, the condition of $\Delta P_{\mathrm{NbC}} = 0.25\Delta P_{\mathrm{NbC},ini}$ corresponds to R_{fin} = 10 μm in Fig. 3 and,

therefore, the initial grains are allowed to grow below this pinning pressure according to the analysis shown in Fig. 3. Both positions gradually move from the left to the right-hand side. It is important to note that the growth front of the abnormally large grains approximately coincide with the position of $\Delta P_{\mathrm{NbC}} = 0.25\Delta P_{\mathrm{NbC},ini}$. Therefore, this value is regarded as a critical value of ΔP_{NbC} in this case at which the coarse grains can preferentially grow. Note that the grain growth from the initial grain structure is completely suppressed without the carburization in this case. Therefore, the grain size remains as the initial value (10 μm) in the whole region except for the AGG region, which allows for a simple estimation of the critical value of $\Delta P_{\mathrm{NbC}} = 0.25\Delta P_{\mathrm{NbC},ini}$ from Fig. 3. However, when the fine grains ahead of AGG region grow, the critical value of ΔP_{NbC} cannot readily be estimated. The critical value must depend on the initial grain structure, the temperature and steel composition. It is important to clarify such dependences and it remains as an important future work.

Next, we investigate the effects of carburization temperature and alloy concentration on the occurrence of AGG. Figure 6 shows the grain structures after carburization at different temperatures, (a) $T = 1000\,^{\circ}\mathrm{C}$ and (b) $T = 950\,^{\circ}\mathrm{C}$ for 1500 s. In Fig. 6(a), coarse grains develop from the left-hand side. Namely, AGG occurs at $T = 1000^{\circ}\mathrm{C}$. However, the growth depth of AGG region at $T = 1000^{\circ}\mathrm{C}$ is obviously smaller than the one at $T = 1050^{\circ}\mathrm{C}$ (Fig.4(d)). This is because f_{NbC} increases with decrease in the temperature and also the carburization is slower at lower temperature. The grain growth is completely inhibited during the carburization at $T = 950^{\circ}\mathrm{C}$, as shown in Fig. 6(b). Figure 7 shows the grain structure after carburization at $T = 1050^{\circ}\mathrm{C}$ for 1500 s in the steel with addition of Al. More specifically, Al composition in the steel was increased from 0.03 mass% to 0.05 mass%. In Fig. 7, some coarse grains appear and the grains near $x = 0$ are relatively large. However, the size of such coarse grains is clearly smaller than the one in Fig. 4. This is because of additional pinning effect due to AlN particle. Although

not shown here, it was found that AGG is completely suppressed by further addition of Al.

As demonstrated above, the present model can simulate AGG during the carburization. It can be utilized for predicting the occurrence of AGG for different carburization condition and different steel compositions.

3.3. Grain growth during the carburization with non-uniform distribution

The microsegregation formed by solidification often causes non-uniform distribution of pinning particles. However, little has been clarified about effects of non-uniform distribution of pinning particles on the grain growth and the occurrence of AGG. In this study, the grain growth during carburization with non-uniform volume fraction of pinning particles is investigated.

For simplicity, we consider non-uniform distribution of volume fraction only in y-direction and it is characterized by two regions; one is the region for high volume fraction and the other is the region for low volume fraction. The pinning pressure in the region for high volume fraction is given as $\Delta P_{\mathrm{pin}} = (1+\Delta f)\beta\sigma\Sigma_i f_i/r_i$ with a constant Δf, while the one in the region for low volume fraction is given as $\Delta P_{\mathrm{pin}} = (1-\Delta f)\beta\sigma\Sigma_i f_i/r_i$. The layers of these regions are alternated at an interval of Δl in y-direction. In this study, several simulations were carried out for different values of Δf and Δl.

Figure 8 shows the microstructures during carburization at T = 1050ºC in a steel with non-uniform distribution of pinning particles for Δf = 0.6 and Δl = 250 μm. The steel composition is the same as the one shown in Fig. 4. The boundaries between low f_v and high f_v regions are indicated by the dashed lines. At t = 500 s, the coarse grains appear only in the low f_v regions and, also, the other grains in low f_v region slightly grow. At t = 1000 s, the further growth of coarse grains is observed in low f_v region and some coarse grains grow toward high

f_v region. This is more obvious in the grain structure at t = 1500 s. It is important to point out that the largest grain observed in Fig. 8 is much larger than the largest grain in Fig. 4. Figure 9 shows the grain structures after carburization at T = 1050°C for 1500 s in a steel with Δf = 0.6 and (a) Δl = 125 μm and (b) Δl = 62.5μm. In both cases, low f_v regions are completely occupied by coarse grains. Also, there is no significant difference in the position of growth front of AGG in both cases. Importantly, as Δl decreases, the high f_v region occupied by the coarse grains increases. Also, the size of coarse grains decreases with decrease in Δl. In other words, when Δl is large, AGG becomes significant.

Figure 10 shows Δl dependence of the ratio of area of low f_v region occupied by coarse grains to total area occupied by coarse grains after the carburization at T = 1050°C for 1500 s. This ratio is a measure of non-uniformity of grain size distribution. A higher value of this ratio indicates the formation of coarser grains as discussed in Figs. 8 and 9. This ratio increases with increases in Δl and/or Δf. Our simulations indicate that significant microsegregation cause the formation of very large coarse grain by AGG during carburization.

In this first attempt to simulate AGG during carburization of steel, we conducted 2D phase-field simulations for the grain growth. Note that the present simulations do not sufficiently carry the quantitative meaning and 3D simulation is necessary in a future work. In addition, it is important to consider the details of precipitation kinetics such as nucleation, dissolution, growth and coarsening of precipitates. This can be achieved by including a more accurate model for precipitation kinetics such as the one developed in Ref. [28] into the present phase-field model. This is also an important future work.

4. Conclusions

In this study, a multi-phase-field model based on the mean field approximation for the

pinning effect is extended to the simulation of abnormal grain growth during carburization in steels. The chief advantage of this model is to explicitly reproduce the curvature-driven growth under the pinning effect and thereby to enable simulations of grain growth under the pinning effects due to very fine particles that are much smaller than the grain size of the matrix. In this study, we have carried out three types of simulations, i.e., grain growth without carburization, grain growth with carburization in steels with uniform and non-uniform distribution of pinning particles. This model can be utilized for understanding and clarifying influences of many factors such as carburization temperature, carburization time, solute concentrations and initial microstructure on the occurrence of AGG. Although we have not considered the details of precipitation kinetics in the present simulations, it is very important for quantitative prediction of AGG to include the kinetics of pinning particles such as the nucleation and growth of carbides, nitrides and carbonitrides during the carburization in detail. This is an important future work.

Acknowledgements

We would like to express our great appreciation to Dr. Kiyotaka Matsuura for his valuable and constructive comments to the present work.

Data availability

The raw/processed data required to reproduce these findings cannot be shared at this time as the data also forms part of an ongoing study.

References

[1] M. Kubota and T. Ochi, Nippon Steel Tech. Rep., 378 (2003), 72.

[2] T. Murakami, H. Hatano and H. Yaguchi, Tetsu-to-Hagané, 92 (2006), 448.

[3] C. Zener, quoted by C. S. Smith, Trans. AIME, 175 (1948),15.

[4] P.A. Manohar, M. Ferry, and T. Chandra, ISIJ Int., 38 (1998), 913-924.

[5] N. Kamiya, Y. Tanaka and R. Ishikura, Daido Steel Tech. Rep., 89(2018), 3.

[6] Y. Yogo and K. Tanaka, Metall. Mater. Trans. A, 45A (2014), 2834.

[7] D.J. Srolovitz, G.S. Grest and M.P. Anderson, Acta metall., 33 (1985), 2233-2247.

[8] Y. Takayama, T. Tozawa, H. Kato and Y. Ushioda, J. Jpn. Inst. Met., 59 (1995), 1006.

[9] K. Shinagawa, S. Maki and K. Yokota, J European Ceram. Soc., 34(2014), 3027.

[10] Y. Suwa, Y. Saito, H. Onodera, Acta Mater., 55 (2007), 6991-6891.

[11] L.-Q. Chen, Annu. Rev. Mater. Res., 32(2002),113.

[12] I. Steinbach, Modelling Simul. Mater. Sci. Eng., 17 (2009), 073001.

[13] N. Moelans, B. Blanpain, P. Wollants, Acta Mater., 53 (2005), 1771-1718.

[14] Y. Suwa, Y. Saito, H. Onodera, Scripta Mater., 55 (2006), 407-410.

[15] C. Schwarze, R. D. Kamachali, and I. Steinbach, Acta Mater, 106(2016), 59.

[16] K. Chang, J. Kwon and C. K. Rhee, Comput. Mater. Sci., 124 (2016), 438.

[17] S. Shahandeh and M. Militzer, Philos. Mag., 93 (2013), 3231.

[18] M. Ohno, Y. Shibuta and T. Takaki, Mater. Trans., 60 (2019), 170.

[19] S. G. Kim, D. I. Kim, W. T. Kim and Y. B. Park, Phys. Rev. E, 74(2006), 061605.

[20] I. Steinbach, F. Pezzolla, Physica D, 134(1999), 385.

[21] T. Takaki, A. Yamanaka and Y. Tomita, ISIJ Int., 51(2011), 1717.

[22] E. Miyoshi, T. Takaki, Y. Shibuta and M. Ohno, Comput. Mater. Sci., 152 (2018), 118-124.

[23] E. Miyoshi, T. Takaki, M. Ohno, Y. Shibuta, S. Sakane, T. Shimokawabe, T. Aoki, npj Compt. Mater., 3 (2017), 25.

[24] C. Bernhard, J. Reiter and H. Presslinger, Metall. Mater. Trans. B, 39B (2008), 885.

[25] M. Hillert, Acta Metall., 12(1965), 227.

[26] K. Banerjee, M. Militzer, M. Perez and X. Wang, Metall. Mat. Trans. A, 41(2010), 3161.

[27] P. W. Voorhees, J. Stat. Phys., 38(1985), 231.

[28] T. Takamiya and O. Furukimi, Tetsu-to-Hagané, 100(2014), 67.

[29] T. Kikutake, Y. Tokunaga, H. Nakao, K. Ito and S. Takaishi, Tetsu-to-Hagané, 5 (1988), 95.

[30] G. Couturier, R. Doherty, C. Maurice and R. Fortunier, Acta Mater., 53(2005), 977.

Table 1 Composition of Nb-added steel investigated in this study

Element	C	Al	Nb	N	Fe
mass%	0.20	0.03	0.05	0.03	Bal.

Table 2 Values of parameters employed in this study.

Parameter	Value
T [ºC]	1050, 1000, 950
σ [J/m^2]	0.79 [18]
$r_{NbC,0}$ [nm]	10
k_{NbC} [m^3/s]	2.364× 10^{-28} [2]
$r_{AlN,0}$ [nm]	40
k_{AlN} [m^3/s]	1.79 × 10^{-24} [29]
β [-]	3.3 [30]
R_{ini} [μm]	5, 10, 15
C at x = 0 [mass%]	1.50

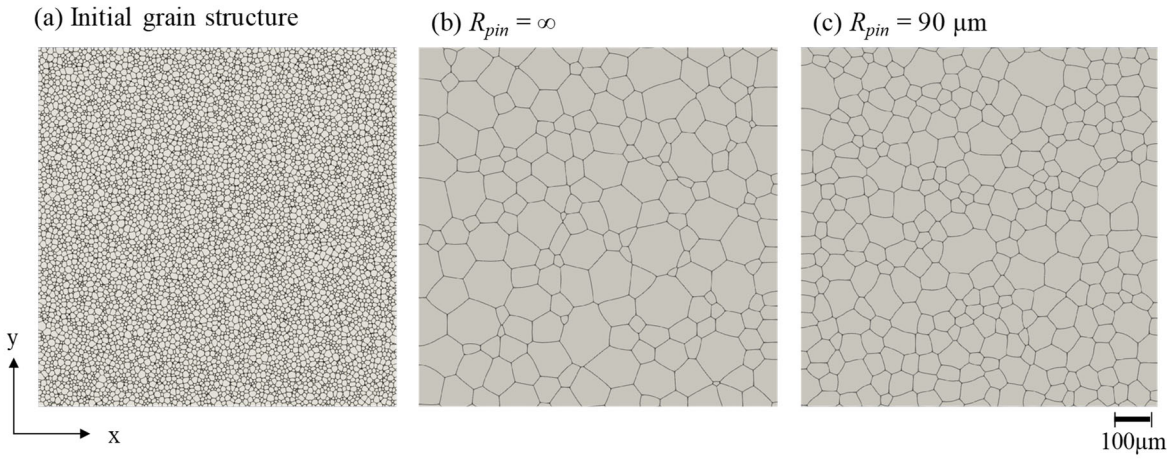

Fig. 1 (a) Initial grain structure and grain structures simulated for (b) $R_{pin}=\infty$ and (c) R_{pin}= 90 μm after isothermal holding for t =13 s at T=1050℃.

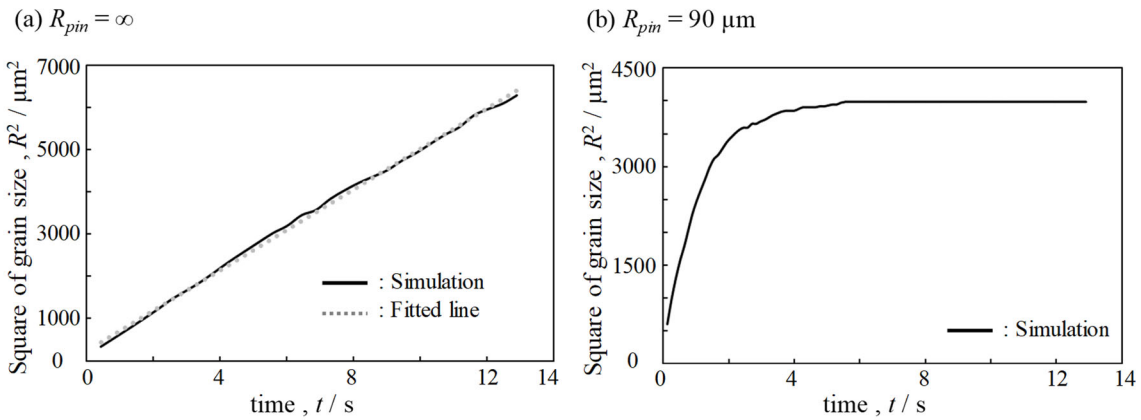

Fig. 2 Time changes of grain size calculated for (a) R_{pin}=∞ and (b) R_{pin}= 90 μm.

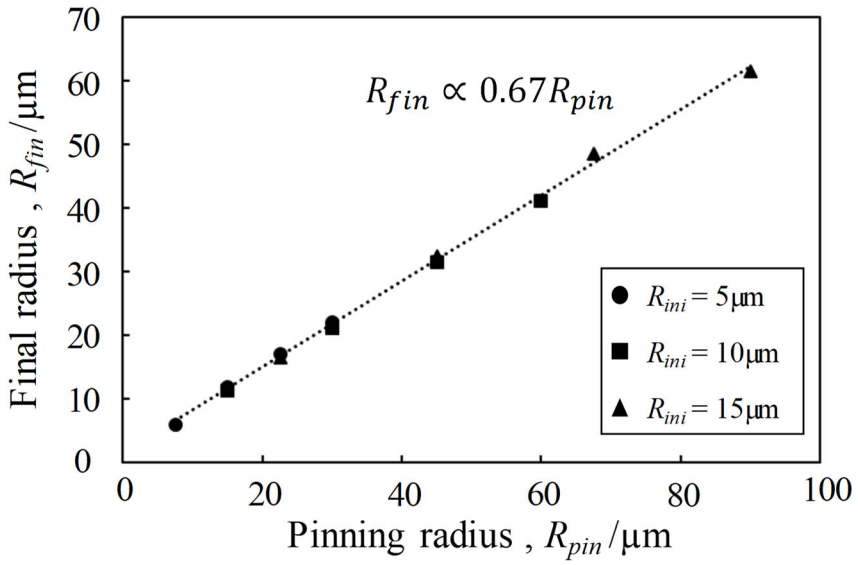

Fig. 3 The relationship between final radius and pinning radius.

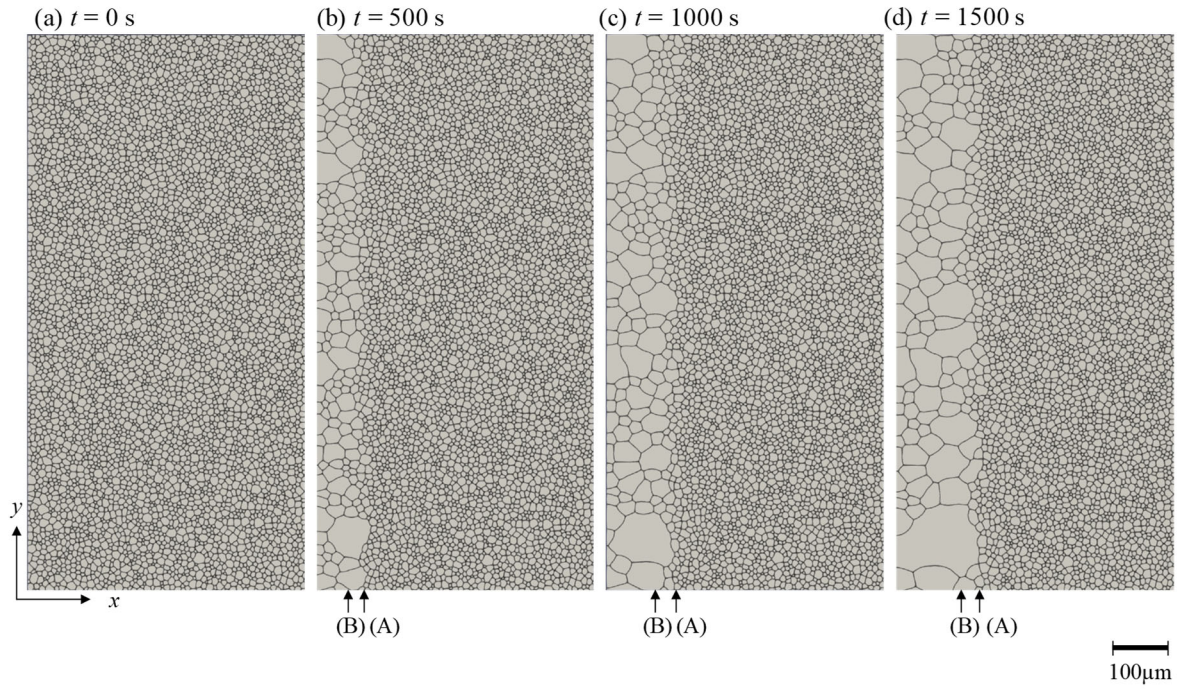

Fig. 4 Grain structures at (a) t = 0 s, (b) t = 500 s, (c) t = 1000 s, (d) t = 1500 s during carburization at T = 1050ºC. The positions where (A) $\Delta P_{\mathrm{NbC}} = 0.25\ \Delta P_{\mathrm{NbC},ini}$ and (B) $\Delta P_{\mathrm{NbC}} = 0$ are indicated by the arrows.

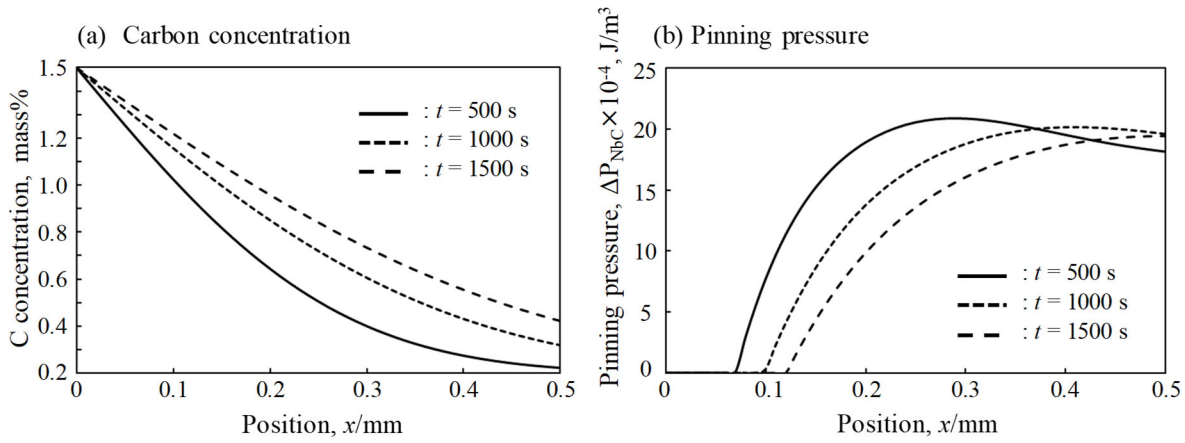

Fig. 5 Spatial profiles of (a) carbon concentration and (b) pinning pressure of NbC at different time steps.

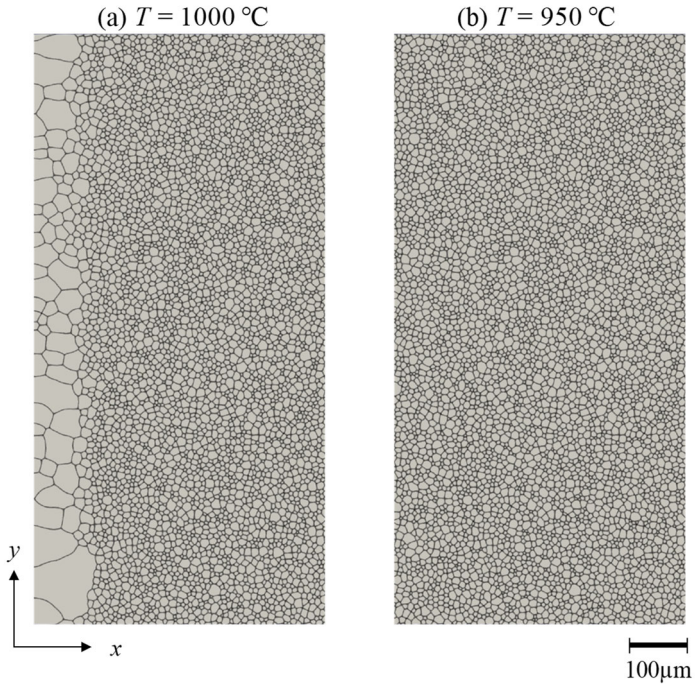

Fig. 6 Grain structures after carburization for t =1500 s at (a) T = 1000℃ and (b) T = 950℃.

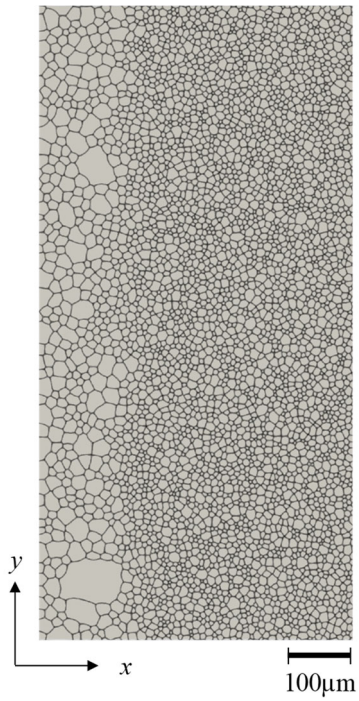

Fig. 7 Grain structure after carburization at T = 1050℃ for t =1500 s in steel with addition of 0.02 mass%Al.

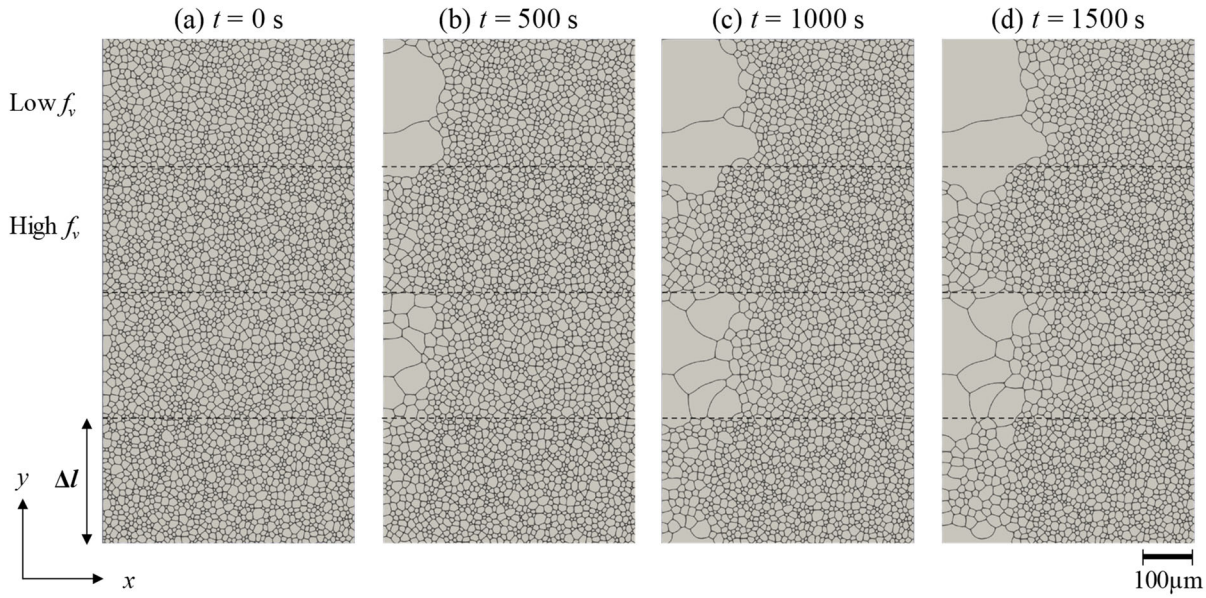

Fig. 8 Grain structures at (a) t = 0 s, (b) t = 500 s, (c) t = 1000 s and (d) t = 1500 s during carburization at T = 1050℃ in a steel with non-uniform distribution of pinning particles calculated for Δl =250 μm and Δf =0.6.

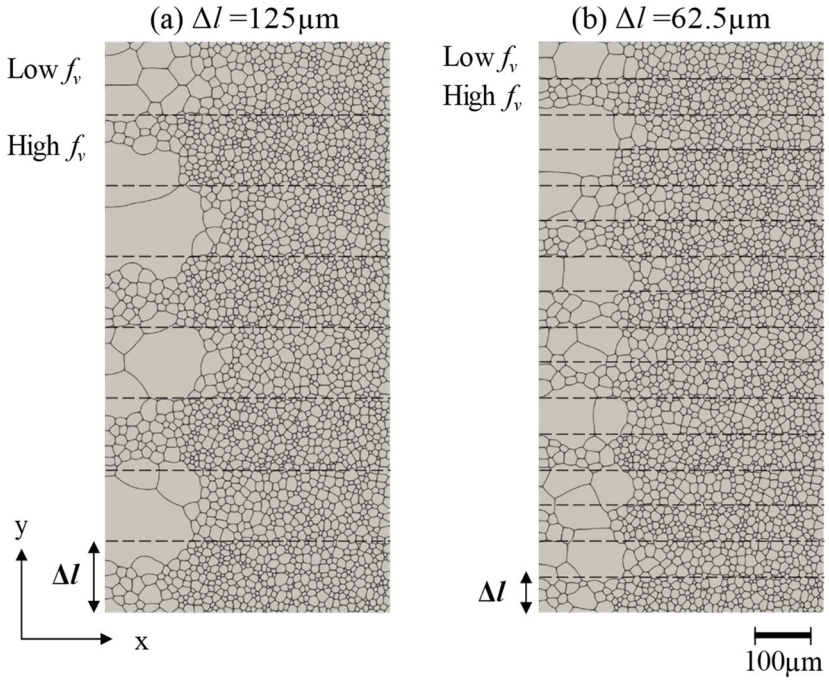

Fig. 9 Grain structures after carburization at T = 1050℃ for 1500 s calculated for (a) Δl =125 μm and (b) Δl =62.5 μm.

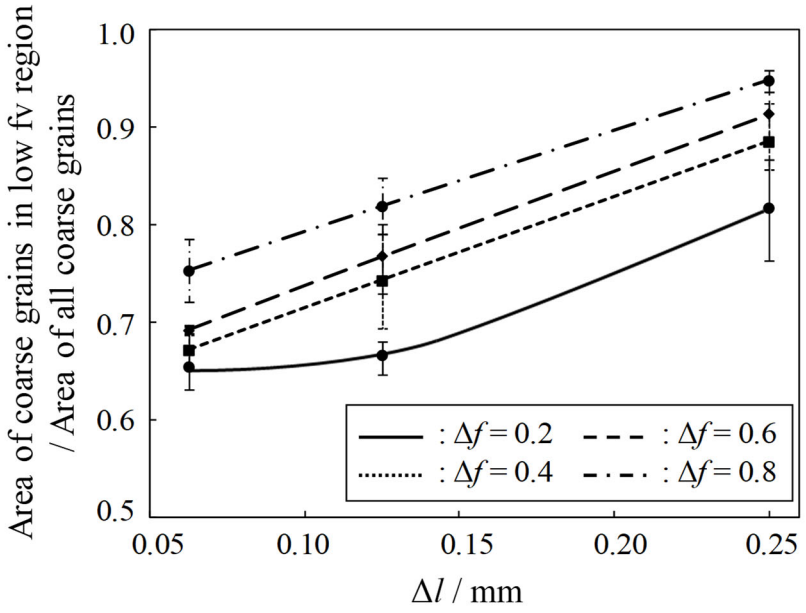

Fig. 10 Summary of results calculated for non-uniform distribution of pinning particles.